Optics Letters

Polarization-independent plasmonic absorption in stacked anisotropic 2D material nanostructures

Sheng-Xuan Xia,[1,2] Xiang Zhai,[1] Ling-Ling Wang,[1] and Shuang-Chun Wen[1,*]

[1]Key Laboratory for Micro/Nano Optoelectronic Devices of Ministry of Education & Hunan Provincial Key Laboratory of Low-Dimensional Structural Physics and Devices, School of Physics and Electronics, Hunan University, Changsha 410082, China
[2]e-mail: shengxuanxia@hnu.edu.cn
*Corresponding author: scwen@hnu.edu.cn

Received 7 November 2019; accepted 18 November 2019; posted 20 November 2019 (Doc. ID 382649); published 18 December 2019

Here we study the possibility to achieve polarization-independent optical absorption in stacked anisotropic 2D material nanostructures (NSs). Focusing on black phosphorus, we demonstrate that by crossly stacking even-layered NSs, surface plasmons resonant in the two lattice directions are complementary excited, leading to polarization-independent absorption at any layer distance. This property is numerically validated using full electromagnetic simulations and theoretically predicted by a two-particle model. Our proposal can open up the possibility of anisotropic 2D materials to develop polarization-independent plasmon devices such as sensors and absorbers.

https://doi.org/10.1364/OL.45.000093

The rise of graphene in the past years has triggered enormous attention on two-dimensional (2D) materials [1,2]. Due to their atomic-scale thicknesses and exotic electronic properties such as ultrahigh charge carrier mobility [3], 2D materials exhibit a variety of exciting optical properties [4]. Among them, strong light-matter interactions, especially surface plasmons, have been widely studied in recent years because of their strong field confinement, as well as low propagation loss [5]. However, due to their various atomic structures and different lattice symmetries, 2D materials mainly provide two distinguishable platforms to support plasmon resonances [6]. The first kind is represented by graphene, which is featured by an in-plane isotropic optical conductivity tensor in all frequencies (that is, $\sigma_{xx} = \sigma_{yy}$, with σ being the conductivity) [2,7]. The other kind is orientation-dependent in-plane anisotropic ones, characterized by an anisotropic optical conductivity tensor (that is, $\sigma_{xx} \neq \sigma_{yy}$) [2]. After years of development, anisotropic 2D materials have become one of the most attractive research fields [5]. This is mainly because they show much richer physics than other 2D materials, e.g., anisotropic plasmons and linear dichroism [8], which adds an additional degree of freedom for adjusting the optical properties of the materials. Among the newly emerged anisotropic 2D material family, the most notable one is black phosphorus (BP). Apart from its pure in-plane anisotropic properties and extraordinary tunability of its optical and electronic properties by means of electrostatic gating and mechanic strain [9] and pressure [10], BP also suggests its potential as a natural hyperbolic material (that is, $\mathrm{Im}(\sigma_{xx} \cdot \sigma_{yy}) < 0$) [2], offering a new platform for modulating 2D surface plasmons [5]. These unique anisotropic and hyperbolic properties have been proved to benefit many polarized applications such as photoluminescence [5], absorption [11,12], sensing [13], and other optoelectronic devices [14]. However, previous anisotropic 2D material-based studies are focused on the strong anisotropy related properties or applications; whether or not they have polarization-independent behaviors that are found to exist only in isotropic 2D materials is still unknown.

In this Letter, we discuss more possibilities of anisotropic 2D materials beyond anisotropic response by using vertically stacked nanostructures (NSs) to achieve polarization-independent optical absorption in a pure anisotropic region. We make BP as a proof-of-concept to demonstrate that when two layers of BP NSs are designed with crossed (same) crystal orientations; the transmitted wave is highly polarization-independent (dependent). Those particular optical phenomena are simulated by using Lumerical FDTD Solutions and can be well explained by applying a two-particle model. Besides, we will reveal that the conclusions can be further extended to stacked NSs with even and odd layers. Finally, the potential applications as polarization-independent refractive sensor and absorber will be discussed.

We first discuss the conductivity of BP in the range of interest. Here the optical properties of a monolayer BP are described by employing a simple semi-classical Drude model, from which the conductivity and the relative permittivity tensor can be calculated; full details can be found in Ref. [15]. Figure 1(a) plots the real and imaginary parts of BP conductivities in the zigzag (ZZ) and armchair (AC) directions. It is obvious that both the real and imaginary parts are always different from each other, and they keep $\mathrm{Im}(\sigma_{ZZ} \cdot \sigma_{AC}) > 0$, meaning that the optical property is pure anisotropic in the considered range. Figure 1(b) shows the propagation of plasmons excited by a dipole at a wavelength of 8 μm, conforming this anisotropy in the two lattice directions.

To make full use of this anisotropy, we design two vertically stacked BP NSs with different lattice direction combinations. The first case is stacked with both ZZs along the x axis [ZZ-ZZ, Fig. 1(c)], whereas the second case is stacked with ZZ/AC in the upper/lower layer along the x axis [ZZ-AC, Figs. 1(d)–1(f)].

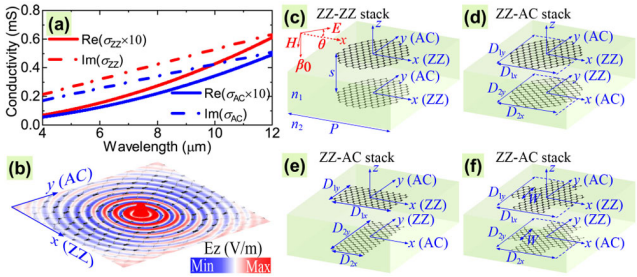

Fig. 1. (a) BP conductivity versus wavelength. (b) Electric z-component of the anisotropic plasmons excited by a dipole located 10 nm above the surface of BP. Structures of one unit of the proposal system with (c) ZZ-ZZ and (d) and (e) ZZ-AC stacks with (c) and (d) elliptic, (e) rectangular, and (f) cross-shaped shapes, respectively.

A schematic layout of the unit cells of our proposal, including all geometrical parameters, is shown in Figs. 1(c)–1(f). These parameters are fixed unless otherwise specified: $D_{li} = 100$ nm (with $l = 1,\ 2$ is layer order, $i = x,\ y$), $P = 200$ nm, and $s = 200$ nm. The dielectric constants are set to $n_1 = n_2 = 1.5$ for the simplicity without loss of generality.

To start with, we first concentrate on the case of BP nanodisks (NDs). Before going further, it is necessary to exploit the supported localized plasmon resonance for the situation with only a one-layer NDs, of which the absorption spectra with ZZ crystal orientation along the x axis for all polarization angles θ are shown in Fig. 2(a). Due to the anisotropic optical property of BP, both the absorption maximum and resonant wavelength are strongly dependent on the excitation direction. There are two dominant absorption peaks at different polarizations, which correspond to the dipole mode resonances in the ZZ and AC directions. When light is polarized in the x direction ($\theta = 0°$), we obtain a high absorption resonance peak. For y polarization ($\theta = 90°$), the resonance shifts to a shorter wavelength as expected due to lower effective mass along the AC (y) direction [15]. Interestingly, for $\theta \sim 45°$, localized plasmons in both ZZ and AC directions are excited simultaneously in smaller intensity due to reduced light intensity at corresponding directions.

Similar anisotropic absorption is also found for the ZZ-ZZ case, as shown in Fig. 2(b). It clearly shows that both the resonant strength and wavelengths are strongly dependent on θ. Compared with Fig. 2(a), the resonance wavelengths are kept the same (that is 8.48 and 7.62 μm for $\theta = 0°$ and 90°, respectively) because the lattice is oriented in the same direction, and the interlayer coupling is not strong enough to push the resonant wavelengths to shorter positions due to the large interlayer distance (e.g., the resonant wavelengths for $s = 30$ nm are 7.65 and 6.88 μm for $\theta = 0°$ and 90°, respectively).

However, different from ZZ-ZZ case, the optical transmission of the ZZ-AC case is totally polarization-independent, as shown in Fig. 2(c). It plainly demonstrates that both the absorption maximum, and resonant wavelength of the two peaks are independent of θ. Notably, the two resonant wavelengths are the same as those of the ZZ-ZZ case because of the weak interlayer couplings. In order to gain more physical insight into the polarization-independent absorption behavior, we plot the field distributions of the plasmons for $\theta = 0°$ in the insets of Fig. 2(d). We find that the absorption at longer wavelength is mainly attributed to the dipole plasmon resonance at the ZZ direction in the upper layer, whereas the shorter one is mainly

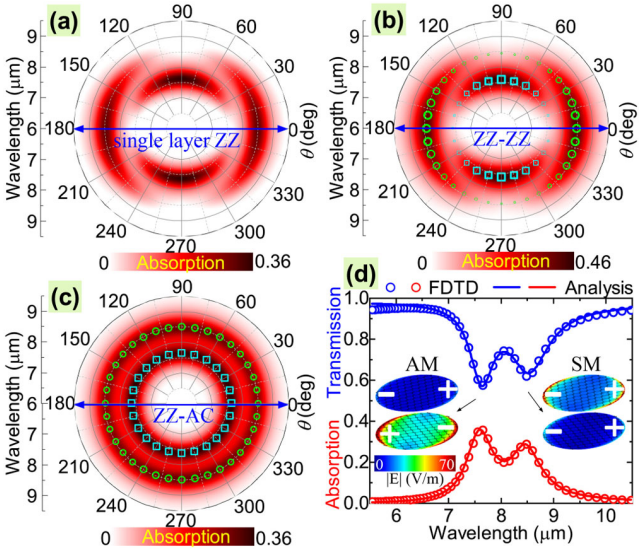

Fig. 2. Absorption maps for the situations with (a) single layer and two-layer BP NDs with (b) ZZ-ZZ and (c) ZZ-AC stack, respectively. The circles/squares indicate the fitted resonant wavelengths of the SM/AM, respectively, with symbol areas proportional to absorption maximum. (d) Absorption and transmission spectra for the ZZ-AC case at $\theta = 0°$. The solid curves and circles represent the analytical and numerical results, respectively. The insets show $|E|$ fields at the SM and AM. The signs "+" and "−" represent the resonating surface charges.

caused by the dipole resonance at the AC direction in the lower layer, forming a symmetric mode (SM) and antisymmetric mode (AM). This is much different from the ZZ-ZZ case where the two BP layers are always resonant at the same position. Therefore, the absorption of the ZZ-AC case is comparable to a single-layer ND, but smaller than the ZZ-ZZ case, as shown in Fig. 2. We note here that the isotropic plasmonic response of a single- or two-layer BP is much different from that of an isotropic graphene, where there is only one absorption peak for both the single- and two-layer cases, though its optical transmission is independent of polarization direction.

To formally demonstrate the physical mechanism of the optical response in the stacked system, we employ two-particle model in the two coordinate axes to theoretically analyze the effective coupling by the following set of equations [16]:

$$a''_{li}(t) + \gamma_{li} a'_{li}(t) + \omega_{li}^2 a_{li}(t) + \kappa_{ll'i}^2 a_{l'i}(t) = Q_{li} E f_{li}(\theta)/m_{li}. \quad (1)$$

Here $f_{lx}(\theta) = \cos(\theta)$, $f_{ly}(\theta) = \sin(\theta)$, γ_{li}, ω_{li}, Q_{li}, and m_{li}, respectively, are the loss factors, resonance frequencies, effective charges, and effective masses of the particles in corresponding layers and lattice orientations. $\kappa_{ll'i}$ defines the coupling strength between the layers. We consider that all particles interact with the incident electric field $E = E_0 e^{i\omega t}$, forming the displacement vectors $a_{li} = c_{li} e^{i\omega t}$. After some algebraic calculations based on Eq. (1), the mode amplitudes of resonators can be obtained:

$$a_{li}(t) = \frac{\kappa_{ll'i}^2 Q_{l'i}/m_{l'i} + \left(\omega^2 - i\omega\gamma_{l'i} - \omega_{l'i}^2\right) Q_{li}/m_{li}}{\kappa_{ll'i}^2 \kappa_{l'li}^2 - \left(\omega^2 - i\omega\gamma_{li} - \omega_{li}^2\right)\left(\omega^2 - i\omega\gamma_{l'i} - \omega_{l'i}^2\right)} \times E f_i(\theta). \quad (2)$$

The effective electric susceptibility (χ_{eff}), which relates the total polarizability (P) of the resonators to the strength of the incident electric field, then can be written as $\chi_{\text{eff}} = P/\varepsilon_0 E$, where $P = (P_x^2 + P_y^2)^{1/2}$, with $P_i = Q_{1i} \cdot a_{1i} + Q_{2i} \cdot a_{2i}$. By using Eqs. (1) and (2), P_i can be expressed as $P_i = \Phi_i E f_i(\theta)$ with

$$\Phi_i = \frac{[\kappa_{21i}^2 Q_{1i} Q_{2i}/m_{1i} + (\omega^2 - i\omega\gamma_{2i} - \omega_{2i}^2) Q_{1i}^2/m_{1i} + \kappa_{12i}^2 Q_{1i} Q_{2i}/m_{2i} + (\omega^2 - i\omega\gamma_{1i} - \omega_{1i}^2) Q_{2i}^2/m_{2i}]}{\kappa_{12i}^2\kappa_{21i}^2 - (\omega^2 - i\omega\gamma_{1i} - \omega_{1i}^2)(\omega^2 - i\omega\gamma_{2i} - \omega_{2i}^2)}. \quad (3)$$

Then the simulated transmission and absorption lines can be fitted by the imaginary part of the susceptibility. In this Letter, they are defined as $T = 1 - \text{Im}(\chi_{\text{eff}})$ and $A = \text{Im}(\chi_{\text{eff}})$ [16].

For the ZZ-AC case, we have $\gamma_{1x} = \gamma_{2y}$, $\gamma_{2x} = \gamma_{1y}$, $\omega_{1x} = \omega_{2y}$, $\omega_{2x} = \omega_{1y}$, $\kappa_{12x} = \kappa_{21x} = \kappa_{12y} = \kappa_{21y} = \kappa$, $Q_{1x} = Q_{2y}$, $Q_{2x} = Q_{1y}$, $m_{1x} = m_{2y}$, and $m_{2x} = m_{1y}$. Hence, $\Phi_x = \Phi_y$, and the effective susceptibility is written as

$$\chi_{\text{eff}} = \Phi_i/\varepsilon_0. \quad (4)$$

which indicates that χ_{eff} is independent of θ. Therefore, the polarization-independent absorption in the ZZ-AC case can be understood by looking into excitation efficiency and interactions in the two layers. Considering that the lattice orientations are perpendicular to each other, and the components of polarizability (P_{li}) are proportional to the external field when the θ changes, regardless of whether the polarizability has been enhanced or weakened in the upper layer in one direction (e.g., as a cosine function of θ in the x axis), it will be compensated for by the lower layer in the other direction (e.g., as a sinusoidal function of θ in the y axis). Besides, because the s-dependent coupling is between the ZZ and AC lattices, the coupling strength along the two principle axes is always the same. Therefore, the complementary excitation efficiency and polarization-insensitive interlayer coupling make the system polarization-independent, as shown in Fig. 2(c). Thus, in our design, the orthogonal lattice directions in stacked BP ND are the key to achieve polarization independence. Figure 2(d) shows the agreement between the analytical results (lines), and the numerical results (circles) are nearly perfect.

For the ZZ-ZZ case, we have $\gamma_{1x} = \gamma_{2x}$, $\gamma_{1y} = \gamma_{2y}$, $\omega_{1x} = \omega_{2x}$, $\omega_{1y} = \omega_{2y}$, $\kappa_{12x} = \kappa_{21x}$, $\kappa_{12y} = \kappa_{21y}$, $Q_{1x} = Q_{2x}$, $Q_{1y} = Q_{2y}$, $m_{1x} = m_{2x}$, and $m_{1y} = m_{2y}$; thus, $\Phi_x \neq \Phi_y$, and the effective susceptibility is written as

$$\chi_{\text{eff}} = \sqrt{\Phi_x^2 \cos^2(\theta) + \Phi_y^2 \sin^2(\theta)}/\varepsilon_0. \quad (5)$$

Equation (5) means the excitation efficiency in the two layers is highly polarization-dependent, as shown in Fig. 2(b).

In the previous sections, we have proved the polarization-independent optical absorption in stacked BP NDs with a large coupling distance; now we will further show that this property is independent of the layer distance. Figure 3(a) shows absorption spectra for different interlayer separations s at $\theta = 0°$. This depicts that as we increase s, the coupling strength decreases monotonically, as shown in the right axis of Fig. 3(a). The decreased coupling further leads to the blueshift and increased resonant strength of the SM, as well as the redshift and decreased resonant strength of the AM, resulting in the two modes approaching each other. At a sufficiently large separation (e.g., > 100 nm), the two layers are almost uncoupled because each layer is well beyond the decay length of the evanescent diffraction field of the other layer. Though both of the resonant wavelengths and strengths of the two modes are tuned by the coupling distance, we have examined (not shown here) that the optical absorption is always independent of θ, no matter how close or far the coupling distance is. This is because the interlayer coupling in the ZZ-AC stacked system is always between the ZZ and AC lattice directions in the two resonant axes. The fitted symbols in Fig. 3(a) show good agreement with the simulated results. Besides, we also simulate the absorption spectra of the situations with only the upper disk (UD) and lower disk (LD) at $\theta = 0°$ and 90°, respectively, finding that when the plasmon reaches its maximum in one layer, the plasmon in the other layer at the same resonant wavelength can also be excited, but with a relative lower strength. This can well explain why we still observe the plasmon field distributions in the two layers simultaneously; even the two layers are

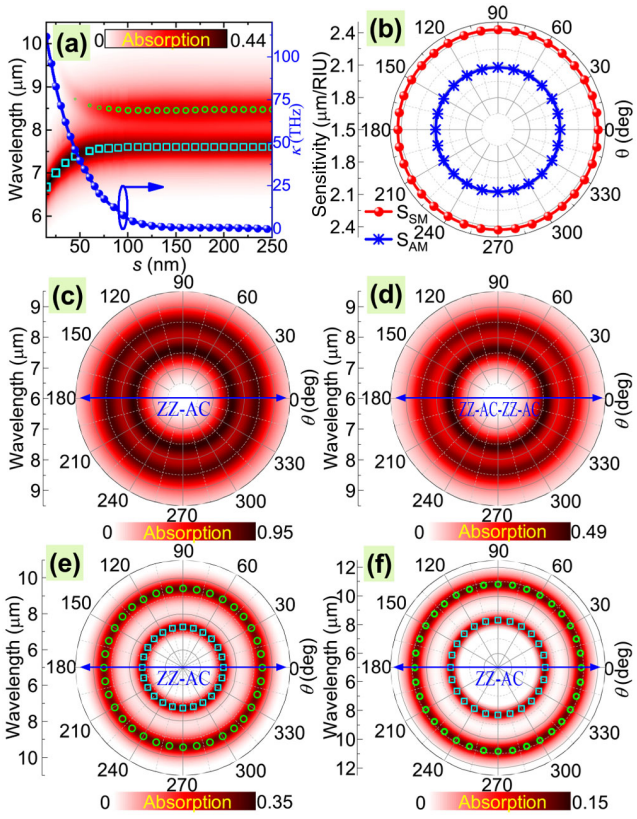

Fig. 3. (a) 2D plot of absorption spectra with $\theta = 0°$ as functions of s and wavelength. The right axis shows the fitted coupling strength. (b) Refractive index sensitivities of the ZZ-AC stacked case. Absorption maps of (c) and (d) disk-, (e) rectangle-, and (f) cross-shaped BP NSs with (c), (e), and (f) ZZ-AC and (d) ZZ-AC-ZZ-AC stacks (c) with and (d)–(f) without a metal substrate, respectively. (e) and (f), respectively, correspond to Figs. 1(e) and 1(f) with $D_{1x} = D_{2y} = 100$ nm, $D_{1y} = D_{2x} = 80$ nm, and $W = 20$ nm. The circles and squares indicate the analytically fitted results, and the symbol areas are proportional to the absorption maximum.

well beyond the decay length of each other (see the insets of Fig. 2(d)).

Now we turn to discuss the potential applications of our design. First, it can be used to design a polarization-insensitive refractive sensor, as shown in Fig. 3(b). We calculate the sensitivities of the two modes by changing n_2 from 1.0 and 1.1. The sensitivity is defined as $S = \Delta\lambda/\Delta n$, specifying the plasmon wavelength shift per refractive index unit (RIU). We find that $S_{\mathrm{SM}} = 2.43$ μm/RIU, and $S_{\mathrm{AM}} = 2.08$ μm/RIU when $s = 200$ nm. These values are higher than some other graphene-based sensors [17,18]. Besides, we also exploit how the coupling distance affects the sensitivities: the smaller the distance is, the lower (higher) is the sensitivity of the SM (AM) (e.g., when $s = 30$ nm, $S_{\mathrm{SM}} = 2.18$ μm/RIU, and $S_{\mathrm{AM}} = 2.52$ μm/RIU). This is because the sensitivity is positively related to the local plasmonic field [18], and a small interlayer distance will lead to a weaker (stronger) resonance of the SM (AM), as shown by Fig. 3(a). In a practical case, this polarization-independent sensor can be maintained by covering the BP nanostructures with hBN layers to increase the stability of BP.

Secondly, the two-layered system can also be used as dual-band polarization-insensitive absorber. After adding a metallic substrate with a 1.1 μm distance below the lower layer ND, the dielectric layer between the BP layers and metallic mirror forms a Fabry−Perot cavity and, thus, increases the interaction of incidence with BP layers, pushing the absorptivity of the two modes to more than 95% in all polarizations, as can be seen in Fig. 3(c). Note that the two polarization-independent absorption peaks are the result of the simultaneously excitation of the dipole plasmons in both the ZZ and AC lattice directions, which is much different from the BP nanoribbon-based metamaterial absorber with second-ordered absorption peaks [19], where the absorption is attributed to four-fold rotational symmetry.

Moreover, we demonstrate that our conclusions can be further extended to other even-layered crossly stacked BP NSs beyond a disk shape. As shown in Fig. 3(d), the ZZ-AC-ZZ-AC stacked four layers are polarization-independent. We have examined that the cases with even- (odd-) layered crossly stacked NDs are all polarization-independent (dependent). Besides, we have further examined that this plasmonic property is not limited to the circular shape; it is entirely general for any other crossly stacked BP NSs. e.g., for rectangle- and cross-shaped BP NSs with $D_{1x} = D_{2y} = 100$ nm and $D_{1y} = D_{2x} = 80$ nm, the absorptions are all polarization-independent, as shown in Figs. 3(e) and 3(f). We also find that this property exists in NSs such as nanoellipses, nanorings, and nanoribbons, *et al.*, providing that the even-layered NSs are crossly stacked and the condition $D_{li} = D_{l'i'}$ is satisfied, which will greatly benefit the practical design of the devices. This is understandable because the excitation efficiencies along the two principle axes are always complemental, meaning that Eq. (4) is always guaranteed.

Finally, we discuss some issues that may arise in a practical application of the proposed structure. The physical mechanism of our proposal requires the upper layer NSs to be vertically aligned and directly above the lower layer to form a stacked ZZ-AC fashion. To show that our construction is experimentally accessible and can be applied to practical devices, we have verified (by using ND) that our proposal has good robustness to geometrical (as shown before) and positional perturbations. For example, when the upper layer ND is oriented with a 5° (10°) rotation to the lower layer, the change of maximum absorptions is only up to 4.90% (10.98%). However, for translational shift, the variations of maximum absorptions just reach 5.68% (10.87%) and 5.27% (7.80%) when the upper layer ND shift for 25 (40) and 10 nm (15 nm) in the axial and catercornered directions, respectively. Notably, the resonant wavelengths of the two modes are always kept the same for all θ for the cases with positional shifts along with the axial directions and with relative rotation of the lattice direction, and they are only slightly affected in the cases with non-axial shifts.

In conclusion, we have made BP as a proof-of-concept to demonstrate that polarization-independent optical absorption can be achieved in anisotropic 2D materials by using two layers of stacked NSs with crossed lattice directions. This property is also independent of the layer distance and can be extended to other crossly stacked NSs with even layers. By applying two-particle model, this property can be well explained as a result of crossed lattice direction-induced complementary plasmon excitations in the two resonant axes. Our proposal is general for anisotropic 2D material-based NSs and can be utilized to design polarization-independent optical devices such as sensors and perfect absorbers.

Funding. National Natural Science Foundation of China (11847230, 11904096, 61775055, 61835004); China Postdoctoral Science Foundation (2018M642967).

Disclosures. The authors declare no conflicts of interest.

REFERENCES

1. F. H. L. Koppens, T. Mueller, P. Avouris, A. C. Ferrari, M. S. Vitiello, and M. Polini, Nat. Nanotechnol. **9**, 780 (2014).
2. T. Low, A. Chaves, J. D. Caldwell, A. Kumar, N. X. Fang, P. Avouris, T. F. Heinz, F. Guinea, L. Martin-Moreno, and F. Koppens, Nat. Mater. **16**, 182 (2016).
3. M. Xu, T. Liang, M. Shi, and H. Chen, Chem. Rev. **113**, 3766 (2013).
4. P. Masih Das, G. Danda, A. Cupo, W. M. Parkin, L. Liang, N. Kharche, X. Ling, S. Huang, M. S. Dresselhaus, V. Meunier, and M. Drndić, ACS Nano **10**, 5687 (2016).
5. C. Wang, G. Zhang, S. Huang, Y. Xie, and H. Yan, "The optical properties and plasmonics of anisotropic 2D materials," Adv. Opt. Mater., 1900996 (2019).
6. Y. Li, Z. Li, C. Chi, H. Shan, L. Zheng, and Z. Fang, Adv. Sci. **4**, 1600430 (2017).
7. H. V. Nguyen and V. H. Nguyen, Phys. Rev. B **94**, 117401 (2016).
8. F. Xia, H. Wang, D. Xiao, M. Dubey, and A. Ramasubramaniam, Nat. Photonics **8**, 899 (2014).
9. K. T. Lam and J. Guo, J. Appl. Phys. **117**, 113105 (2015).
10. E. van Veen, A. Nemilentsau, A. Kumar, R. Roldán, M. I. Katsnelson, T. Low, and S. Yuan, Phys. Rev. Appl. **12**, 014011 (2019).
11. F. Xiong, J. Zhang, Z. Zhu, X. Yuan, and S. Qin, J. Opt. **19**, 075002 (2017).
12. T. Liu, X. Jiang, C. Zhou, and S. Xiao, Opt. Express **27**, 27618 (2019).
13. G. Lee, S. Kim, S. Jung, S. Jang, and J. Kim, Sens. Actuators, B **250**, 569 (2017).
14. P. Chen, N. Li, X. Chen, W.-J. Ong, and X. Zhao, 2D Mater. **5**, 014002 (2017).
15. Z. Liu and K. Aydin, Nano Lett. **16**, 3457 (2016).
16. F. Meng, Q. Wu, D. Erni, K. Wu, and J. Lee, IEEE Trans. Microwave Theory Tech. **60**, 3013 (2012).
17. S. X. Xia, X. Zhai, L. L. Wang, B. Sun, J. Q. Liu, and S. C. Wen, Opt. Express **24**, 17886 (2016).
18. S. Xia, X. Zhai, Y. Huang, J. Liu, L. Wang, and S. Wen, J. Lightwave Technol. **35**, 4553 (2017).
19. J. Wang, Y. Jiang, and Z. Hu, Opt. Express **25**, 22149 (2017).